Pergamon

Int. J. Heat Mass Transfer. Vol. 40, No. 4, pp. 757–763, 1997

0017–9310/97 $17.00 + 0.00

PII: S0017-9310(96)00153-6

Numerical investigation on a simulation model of floating zone convection

Q. S. CHEN and W. R. HU

Institute of Mechanics, CAS, Beijing 100080, People's Republic of China

(*Received for publication* 21 *May* 1996)

Abstract—A simulation model with adiabatic condition at the upper rod and constant temperature at the lower rod is studied numerically in this paper. The temperature distribution in a simulation model is closer to the one in the half part of a floating full zone in comparison with the one in a usual floating half zone model with constant temperature at both rods, because the temperature distribution of a floating full zone is symmetric for the middle plane in a microgravity environment. The results of the simulation model show that the temperature profiles and the flow patterns are different from those of the usual floating half zone model. Another type of half zone model, with a special non-uniform temperature distribution at the upper rod and constant temperature at the lower rod, has been suggested by recent experiments. The temperature boundary condition of the upper rod has a maximum value in the center and a lower value near the free surface. This modified simulation model is also simulated numerically in the present paper. Copyright © 1996 Elsevier Science Ltd.

1. INTRODUCTION

The floating zone method is of technical importance for the growth of some crystals. Contamination of the dissolution of the crucible can be avoided by using this method. The diameter of the melt column will be limited on earth processing, since the melt volume will be confined by surface tension. The opportunity of accessing a low gravity environment may give the possibility of growing larger crystals of high quality using this method. In order to investigate the thermocapillary convection of a floating zone melting under low gravity, the floating half zone model has been carried out over the past 20 years [1–8] and the usual floating half zone model is confined between two cylindrical rods, where it keeps constant temperatures as shown in Fig. 1a. It has been found that the convection will be steady and axisymmetric if the Marangoni number is smaller than a critical value and the flow becomes oscillatory when a critical Marangoni number is exceeded. The oscillatory flow pattern depends on many critical parameters, including the geometrical parameters such as the aspect ratio and the zone volume.

In order to get more information on floating full zone melting, a simulation model of the floating half zone is suggested, as shown in Fig. 1b, where the temperature at the lower rod remains constant and the upper rod has a nearly zero temperature gradient in a normal direction. The thermal transfer in the upper rod is much slower than that in the liquid bridge, that is

$$\frac{\partial T}{\partial n} = \frac{k_s}{k}\frac{\partial T_s}{\partial n} \to 0, \quad \text{if } k_s \ll k \tag{1}$$

where k, n and T are, respectively, the heat conductivity, normal direction of interface and temperature and subscript s denotes the value of solid. The temperature distribution in this simulation model is more closely related to the one in the half part of a full floating zone. The temperature distribution in a liquid bridge of floating zone will be symmetric for the middle plane in a microgravity environment, so the temperature gradient in the longitudinal direction in the middle plane should be zero. The simulation model of floating zone convection will be studied in detail in the present paper.

A modified simulation model of floating half zone has been suggested experimentally in Waseda University of Japan since the late 1980s [9, 10]. The model configuration is shown in Fig. 1c, where the lower rod consists of copper with a constant temperature and the upper rod consists of sapphire, heated by a heater around the sapphire rod. The transparent material of sapphire is beneficial for optical observation of the flow pattern in the azimuthal direction. The temperature distribution of this model is non-uniform at the upper rod, but the temperature is higher in the central part of the upper rod, because of the higher thermal conductivity of sapphire in comparison with the experimental medium such as silicon oil, as in the case of $k_s \gg k$ in equation (1). Recently, a similar experiment was also developed in Korea [11], in which the model is close to the usual half zone model as shown in Fig. 1a, but not to the simulation model as shown in Fig. 1b and has also been studied in the present paper.

In present numerical studies, the differences in temperature distributions and flow patterns between the usual floating half zone model, simulation model and

NOMENCLATURE

A	aspect ratio, $L/2R_0$
c	Stefan–Boltzmann constant, 5.67×10^{-8} J m^{-2} s^{-1} K^{-4}
i	integer denoting grid station in radial direction, $i=0,1,2,\ldots,M$
j	integer denoting grid station in axial direction, $j=0,1,2,\ldots,N$
k	thermal conductivity of the melt [J m^{-1} s^{-1} K^{-1}]
k_s	thermal conductivity of the rod material [J m^{-1} s^{-1} K^{-1}]
L	the gap between the two rods [m]
M	integer denoting the last grid station in a radial direction
Ma	Marangoni number, $\lvert\sigma_T'\rvert\Delta TL/\rho\nu\alpha$
n	normal direction of the interface
N	integer denoting the last grid station in an axial direction
p	dimensionless pressure in the melt $(P/\rho U_0^2)$
P	pressure in the melt [N m^{-2}]
P_∞	pressure in the surrounding gas [N m^{-2}]
Pr	Prandtl number, ν/α
q	dimensionless total pressure in the melt, $p+(u^2+w^2)/2$
$\tilde{q}$	spectral coefficient of q
q_0	dimensionless pressure at $r=R$, $z=0$
r	dimensionless radial coordinate
R	dimensionless radius of the free surface
R_0	radius of the rod [m]
Rc	radiation number, $\varepsilon cL\Delta T^3/k$
Re	Reynolds number, U_0L/ν
t	dimensionless time
T	temperature [K]
T_m	the mth degree Chebyshev polynomial
T_n	the nth degree Chebyshev polynomial
T_s	temperature of the rod [K]
T_0	temperature at the lower rod [K]
T_∞	temperature of the surrounding gas [K]
ΔT	temperature difference between the upper and lower rods at the free surface
u	dimensionless radial velocity component of the melt, U/U_0
$\tilde{u}$	spectral coefficient of u
U	radical velocity component of the melt [m s^{-1}]
U_0	reference velocity, $\lvert\sigma_T'\rvert\Delta T/\rho\nu$
w	dimensionless axial velocity component of the melt, W/U_0
$\tilde{w}$	spectral coefficient of w
W	axial velocity component of the melt [m s^{-1}]
z	dimensionless axial coordinate.

Greek symbols

α	thermal diffusivity of the melt [m^2 s^{-1}]
δ	heater width on the upper rod in mode b
ε	radiation coefficient
Θ	dimensionless temperature, $(T-T_0)/\Delta T$
$\tilde{\Theta}$	spectral coefficient of Θ
Θ_0	dimensionless temperature distribution on the upper rod in mode c
ν	kinematic viscosity of the melt [m^2 s^{-1}]
ρ	density of the melt [kg m^{-3}]
σ	surface tension [N m^{-1}]
σ_T'	surface tension differentiation with respect to temperature [N m^{-1} K^{-1}].

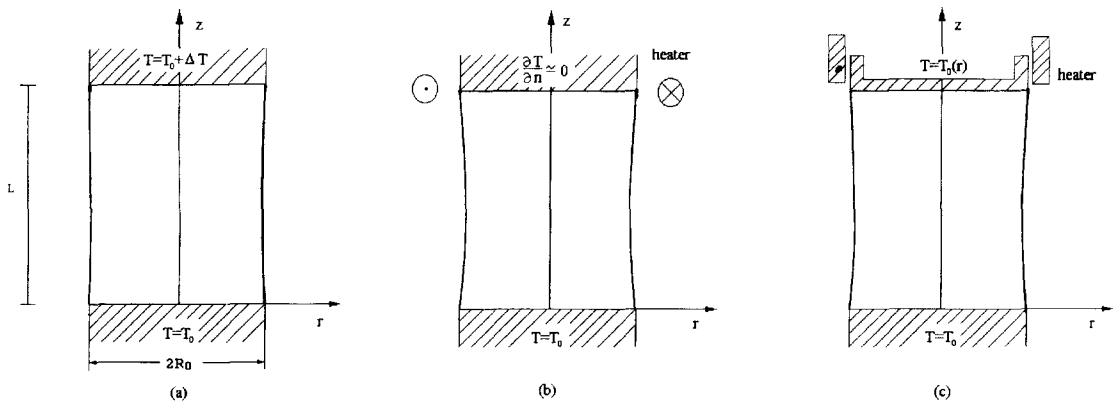

Fig. 1. Configurations of three types of floating half zone models: (a) usual half zone model with constant temperatures on both rods, (b) simulation half zone model with adiabatic condition at the upper rod and constant temperature at the lower rod, and (c) modified half zone model with non-uniform temperature distribution at the upper rod and constant temperature at the lower rod.

modified simulation model were analyzed. The mathematical description is given in Section 2 and then the results of the numerical simulation for three models are discussed in Section 3. Section 4 gives conclusions.

2. THE MATHEMATICAL MODEL

In this paper a precise spectral method is employed to solve the mass, momentum and energy equations. Axisymmetric convective flow was assumed. The Prandtl, Reynolds, Marangoni and radiation numbers and aspect ratio are defined, respectively, as

$$Pr = \frac{\nu}{\alpha}, \quad Re = \frac{U_0 L}{\nu}, \quad Ma = Re \times Pr = \frac{|\sigma_T'|\Delta T L}{\rho \nu \alpha},$$

$$Rc = \frac{\varepsilon c L \Delta T^3}{k}, \quad A = \frac{L}{2R_0}$$

where reference velocity $U_0 = |\sigma_T'|\Delta T/\rho\nu$, L is the gap between the two rods and R_0 is the radius of the rod. ΔT is the applied temperature difference between the upper and lower rods at the free surface. Constants ρ, ν, k, α, ε, c, σ_T' denote density, kinematic viscosity, thermal conductivity, thermal diffusivity, radiation coefficient, the Stefan–Boltzmann constant and surface tension differentiation with respect to temperature. The dimensionless velocities, static pressure and temperature are defined as

$$u = \frac{U}{U_0}, \quad w = \frac{W}{U_0}, \quad p = \frac{P}{\rho U_0^2}, \quad \Theta = \frac{T - T_0}{\Delta T}$$

where U, W, P, T denote dimension velocities in the radial direction and longitudinal direction, pressure and temperature and T_0 is the temperature at the lower rod. The dimensionless time t is obtained by normalizing the time with the tension time scale, L/U_0, the dimensionless radial distance r and axial distance z are obtained by normalizing the respective distances with the reference length scale L. A cylindrical coordinate system is adopted. The governing equations with Bussinesq approximation are as follows:

$$\frac{\partial u}{\partial r} + \frac{u}{r} + \frac{\partial w}{\partial z} = 0 \tag{2}$$

$$\frac{\partial u}{\partial t} + w\left(\frac{\partial u}{\partial z} - \frac{\partial w}{\partial r}\right) = -\frac{\partial q}{\partial r} + \frac{1}{Re}\left(\frac{\partial^2 u}{\partial r^2} + \frac{1}{r}\frac{\partial u}{\partial r} - \frac{u}{r^2} + \frac{\partial^2 u}{\partial z^2}\right) \tag{3}$$

$$\frac{\partial w}{\partial t} - u\left(\frac{\partial u}{\partial z} - \frac{\partial w}{\partial r}\right) = -\frac{\partial q}{\partial z} + \frac{1}{Re}\left(\frac{\partial^2 w}{\partial r^2} + \frac{1}{r}\frac{\partial w}{\partial r} + \frac{\partial^2 w}{\partial z^2}\right) \tag{4}$$

$$\frac{\partial \Theta}{\partial t} + u\frac{\partial \Theta}{\partial r} + w\frac{\partial \Theta}{\partial z} = \frac{1}{Re\,Pr}\left(\frac{\partial^2 \Theta}{\partial r^2} + \frac{1}{r}\frac{\partial \Theta}{\partial r} + \frac{\partial^2 \Theta}{\partial z^2}\right) \tag{5}$$

where q is the total pressure,

$$q = p + \tfrac{1}{2}(u^2 + w^2). \tag{6}$$

When applying the divergence operator to the momentum equations, the Poisson pressure equation is obtained as follows:

$$\left(\frac{\partial^2}{\partial r^2} + \frac{1}{r}\frac{\partial}{\partial r} + \frac{\partial^2}{\partial z^2}\right)q = -\frac{\partial}{\partial t}\left(\frac{\partial u}{\partial r} + \frac{u}{r} + \frac{\partial w}{\partial z}\right) - \left(\frac{\partial}{\partial r} + \frac{1}{r}\right)\left[w\left(\frac{\partial u}{\partial z} - \frac{\partial w}{\partial r}\right)\right] + \frac{\partial}{\partial z}\left[u\left(\frac{\partial u}{\partial z} - \frac{\partial w}{\partial r}\right)\right] + \frac{1}{Re}\left(\frac{\partial^2}{\partial r^2} + \frac{1}{r}\frac{\partial}{\partial r} + \frac{\partial^2}{\partial z^2}\right)\left(\frac{\partial u}{\partial r} + \frac{u}{r} + \frac{\partial w}{\partial z}\right). \tag{7}$$

The free surface shape is determined by the surface tension, gravity, etc. Zero gravity is assumed in the present paper and the dimensionless normal stress equation on the free surface of a static liquid volume is as follows:

$$p = \frac{\sigma}{\rho U_0^2 L}\left[\frac{1}{R(1+R'^2)^{1/2}} - \frac{R''}{(1+R'^2)^{3/2}}\right] + \frac{P_\infty}{\rho U_0^2} \tag{8}$$

where P_∞, σ, R are the pressure in the surrounding gas, the surface tension and the radius of the free surface and the prime $'$ denotes the differentiation of the radius with respect to z. The static pressure and the free surface position in the static isothermal equilibrium with a certain aspect ratio and liquid volume can be obtained by equation (8) with a constant volume constraint. Especially in the present simulation, a cylindrical liquid bridge is adopted with the static pressure

$$p = \frac{\sigma}{\rho U_0^2 R_0} + \frac{P_\infty}{\rho U_0^2}. \tag{9}$$

The free surface position is assumed to be unchangeable during the heating process.

The boundary conditions of velocity and temperature at the upper rod and the lower rod are as follows:

$$z = 0: \quad u = 0, w = 0, \Theta = 0 \tag{10}$$

$$z = 1: \quad u = 0, w = 0 \tag{11}$$

$$\Theta = 1; \quad \text{for model a}$$

$$\begin{cases} \dfrac{\partial \Theta}{\partial z} = 0, & 0 \leqslant r < R(z) - \delta \\ \Theta = 1; & R(z) - \delta \leqslant r \leqslant R(z) \end{cases} \quad \text{for model b} \tag{12}$$

$$\Theta = \Theta_0(r) \quad \text{for model c}$$

where δ is a small positive number and is adopted as the width of the outer part of the upper rod where it keeps constant temperature. The temperature on the lower rod is constant in three models. The temperature conditions on the upper rod are varied according to different floating half zone models as shown in Figs. 1a, b and c, which were defined as model a, model b and model c. Constant temperature distribution at the upper rod is adopted for the usual model a, adiabatic condition for the simulation model b except the outer part of the upper rod where the temperature keeps a higher value in a small region of width δ and a given temperature distribution $\Theta_0(r)$ for the modified simulation model c. In the modified simulation model c, the temperature distribution at the upper rod is chosen as in the experiment, with higher temperature in the center part of the upper rod [9, 10].

The velocity and temperature boundary conditions on the free surface are

$$2\left(\frac{\partial u}{\partial r}-\frac{\partial w}{\partial z}\right)R'+\left(\frac{\partial w}{\partial r}+\frac{\partial u}{\partial z}\right)(1-R'^2)$$
$$=-(1+R'^2)^{1/2}\left(\frac{\partial \Theta}{\partial r}R'+\frac{\partial \Theta}{\partial z}\right) \quad (13)$$

$$u-wR'=0 \quad (14)$$

$$\frac{\partial \Theta}{\partial r}-\frac{\partial \Theta}{\partial z}R'=(1+R'^2)^{1/2}Rc\left(\frac{T_\infty^4-T^4}{\Delta T^4}\right) \quad (15)$$

where T_∞ is the environment temperature in the gas. The boundary conditions at the centerline are chosen as

$$u=0,\frac{\partial w}{\partial r}=0,\frac{\partial \Theta}{\partial r}=0. \quad (16)$$

The method of pressure boundary conditions for the associated Poisson pressure equation proposed by Gresho and Sani [12] is used. The normal component of the momentum equations is used as the pressure boundary condition at both solid boundaries and free surfaces. The pressure boundary conditions are as follows:

$$z=0 \quad \text{and} \quad z=1: \quad \frac{\partial q}{\partial z}=\frac{1}{Re}\frac{\partial^2 w}{\partial z^2}, \quad (17)$$

$$r=R(z): \quad \frac{\partial q}{\partial r}-R'\frac{\partial q}{\partial z}=-\frac{\partial u}{\partial t}-w\left(\frac{\partial u}{\partial z}-\frac{\partial w}{\partial r}\right)$$
$$+\frac{1}{Re}\left(\frac{\partial^2 u}{\partial r^2}+\frac{1}{r}\frac{\partial u}{\partial r}-\frac{u}{r^2}+\frac{\partial^2 u}{\partial z^2}\right)$$
$$-R'\left[-\frac{\partial w}{\partial t}+u\left(\frac{\partial u}{\partial z}-\frac{\partial w}{\partial r}\right)+\frac{1}{Re}\left(\frac{\partial^2 w}{\partial r^2}+\frac{1}{r}\frac{\partial w}{\partial r}+\frac{\partial^2 w}{\partial z^2}\right)\right] \quad (18)$$

$$r=0: \quad \frac{\partial q}{\partial r}=0 \quad (19)$$

and an additional pressure constraint condition is also added to ensure a unique pressure solution, such as

$$r=R,z=0: \quad q=q_0 \quad (20)$$

q_0 is the pressure in the liquid at the lower corner near the free surface and represents the reference pressure. Although q_0 should be determined by constant volume constraint, it is assumed that the free surface shape will not change during the heating process in microgravity and q_0 is chosen as the static pressure in a cylindrical isothermal liquid bridge in equation (9). The reference pressure value q_0 will not influence the solutions of velocities and temperature, since only derivatives of pressure appear in the momentum equations.

The pressure field is obtained by solving the pressure Poisson equation (7), combined with the pressure boundary conditions (17)–(20). The velocity and temperature fields are also obtained by solving the momentum and energy equations (3)–(5) with the boundary conditions (10)–(16). It has been proved that the continuity equation will be automatically satisfied if the initial divergence of velocity is kept zero by using the method above [12].

The spatial discretization is based on a spectral method using Chebyshev polynomial expansions in the axial direction and the radial direction,

$$\begin{Bmatrix} u(r,z) \\ w(r,z) \\ q(r,z) \\ \Theta(r,z) \end{Bmatrix} = \sum_{m=0}^{M}\sum_{n=0}^{N}\begin{Bmatrix} \tilde{u}(m,n) \\ \tilde{w}(m,n) \\ \tilde{q}(m,n) \\ \tilde{\Theta}(m,n) \end{Bmatrix} T_m\left[\frac{2r}{R(z)}-1\right]T_n(2z-1) \quad (21)$$

where M, N are the orders of Chebyshev polynomial expansions in radial and longitudinal directions, respectively. The collocation grids are chosen by

$$(r_i,z_j)=\left[\frac{R(z)}{2}\left(\cos\frac{\pi i}{M}+1\right),\frac{1}{2}\left(\cos\frac{\pi j}{N}+1\right)\right],$$
$$0\leqslant i\leqslant M,0\leqslant j\leqslant N. \quad (22)$$

The algebraic equations are obtained by substituting the variables in the equations and boundary conditions with associated Chebyshev polynomial expansions (21) at each node. The finite difference methods are used for the time integration. The viscous terms are treated implicitly and the non-linear terms explicitly. The non-linear terms are calculated by the pseudospectral approximation [13]. The initial conditions chosen are linear distribution for temperature and zero for velocity. When processing the algorithm, the flow pattern and the temperature distribution will approach equilibrium solutions under the critical Marangoni number. All the results presented hereafter are obtained at dimensionless time $t=1000$ with grid

points of 32×32 and a timestep of 0.005; the environmental temperature and the lower rod temperature are taken as 20°C.

3. RESULTS OF NUMERICAL SIMULATION

The usual half zone model is extensively used to investigate the thermocapillary convection and more details of convective features have been studied both theoretically and experimentally. The convection is steady and axisymmetric if the Marongoni number is smaller than the critical value and these conditions will be discussed in this section. It could be expected that the features of the thermocapillary convection will be determined sensitively by the applied temperature of the floating half zone; different kinds of half zone models associate with different thermal conditions and may induce different profiles of physical quantities. In order to compare the flow pattern variations of different models in the same parameters, the three models have been simulated by using the method mentioned in the last section with $pr = 50$, $Ma = 5000$, $A = 0.7$. In the usual half zone model a, both the upper rod and the lower rod have constant temperature distributions. In the simulation half zone model b, the upper rod has a zero temperature gradient in the normal direction and a small region with width δ of heating part at the upper rod is chosen as one-fifth of the radius of the rod. In the modified half zone model c, the upper rod has a fixed temperature distribution chosen as the one in an experiment [9, 10] and the lower rod maintains a constant temperature. The flow pattern (Fig. 2a) and temperature distribution (Fig. 3a) of the usual half zone model a are in great agreement with the ones obtained in [14] by using the finite element method.

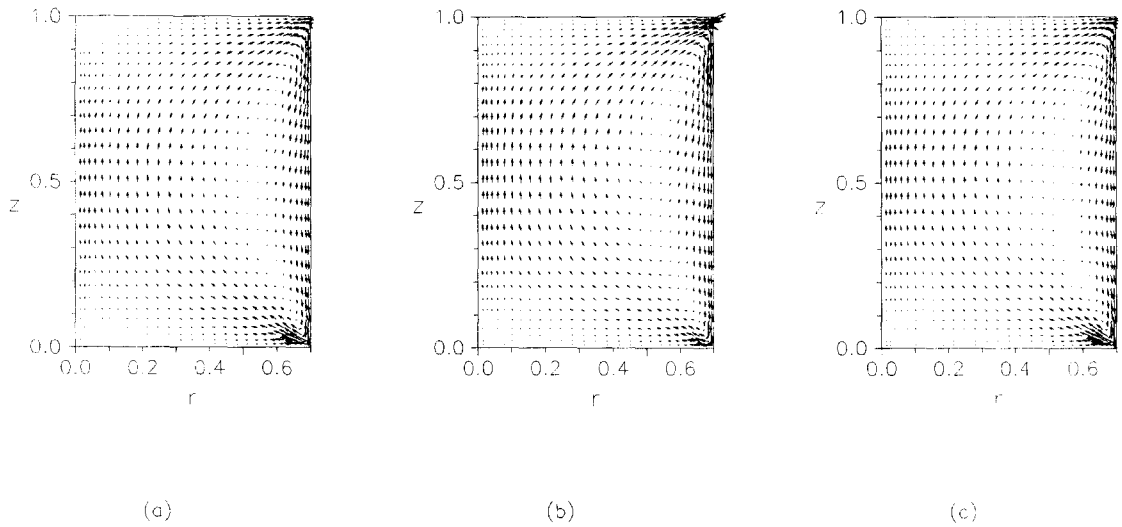

Fig. 2. Velocity patterns in the radial cross-section of half zone with $Pr = 50$, $Ma = 5000$, $A = 0.7$ for: (a) usual half zone model, (b) simulation half zone model and, (c) modified half zone model.

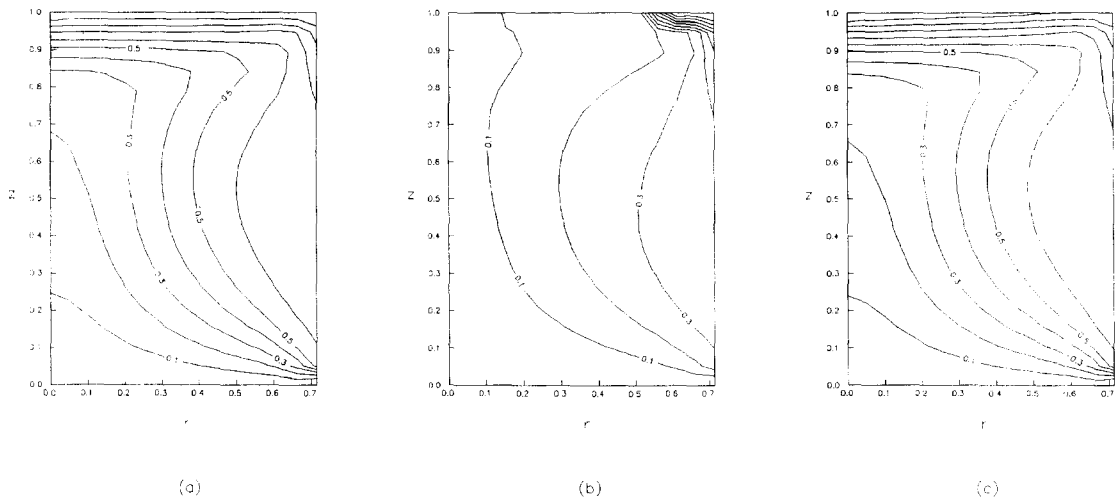

Fig. 3. Isotherms in the radial cross-section of half zone with $Pr = 50$, $Ma = 5000$, $A = 0.7$ for: (a) usual half zone model, (b) simulation half zone model and, (c) modified half zone model.

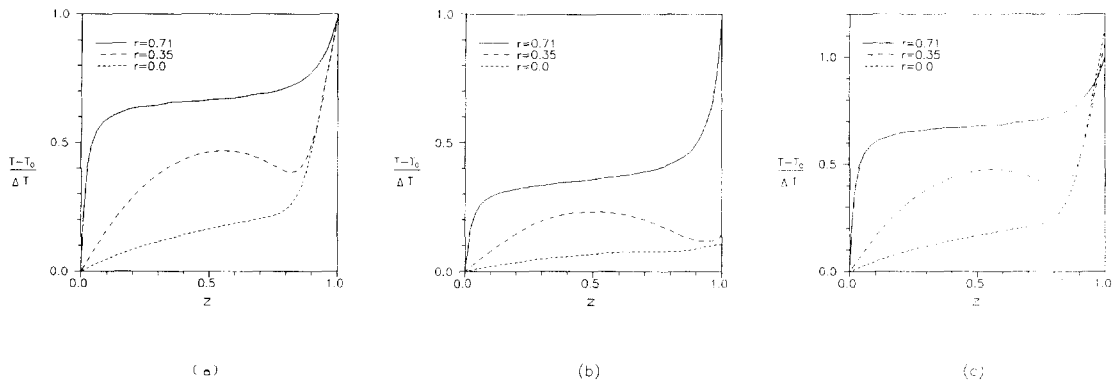

Fig. 4. Temperature profiles along an axial direction with $Pr = 50$, $Ma = 5000$, $A = 0.7$ for: (a) usual half zone model, (b) simulation half zone model and, (c) modified half zone model.

The velocity patterns in radial cross-sections of half zone models have been plotted in Figs. 2a–c for the usual half zone model a, the simulation half zone model b and the modified half zone model c, respectively. Each flow pattern has a steady and axisymmetric roll configuration. The cell center in the simulation half zone model b is higher than the one in both model a and model c. The velocity in the upper corner near the free surface is also larger in the simulation model b than the ones in other models and the velocity in the lower corner near the free surface is relatively lower in the simulation model b. It could be seen that the flow pattern of the modified simulation model c is similar to that of the usual model a, because the temperature non-uniformity at the upper rod is small in model c, although it is a non-uniform temperature distribution.

The isotherm lines of the three models are shown in Figs. 3a–c for the usual half zone model a, the simulation half zone model b and the modified half zone mode c, respectively. In the simulation model as shown in Fig. 3b, zero temperature gradient in the normal direction is required and a relatively lower temperature appears in the center part of the upper rod, while a higher temperature exists in the outer part of the upper rod. The temperature distribution in the simulation half zone model b agrees well with the results obtained by considering a floating full zone [15]. The temperature gradients in both the usual model a and the modified model b have a large value in the center part of the upper rod.

The temperature distribution along the longitudinal direction in different radial distances can be seen in Figs. 4a–c. In both the usual half zone model a and the modified half zone model c, the temperature gradients are larger in the region of the upper part of liquid bridge near the axis and in the corner of the lower rod near the free surface, although there are differences near the upper rod due to different boundary values. On the contrary, the maximum temperature gradient in the longitudinal direction exists in the corners near the surface in simulation model b and the temperature profile is quite flat in the region of the central axis.

The radial temperature distributions at a fixed height can be seen in Fig. 5. The temperature at the upper rod keeps constant in usual model a. Both the simulation half zone model b and the modified half zone model c have non-uniform temperature distribution on the upper rod. However, it can be seen from Figs. 5b and 5c, that the temperature distribution has only a limited difference at $z = 1$ in Fig. 5c and a large difference at $z = 1$ in Fig. 5b and the temperature in the center part of the upper rod is lower in the simulation half zone model b, while it is higher in

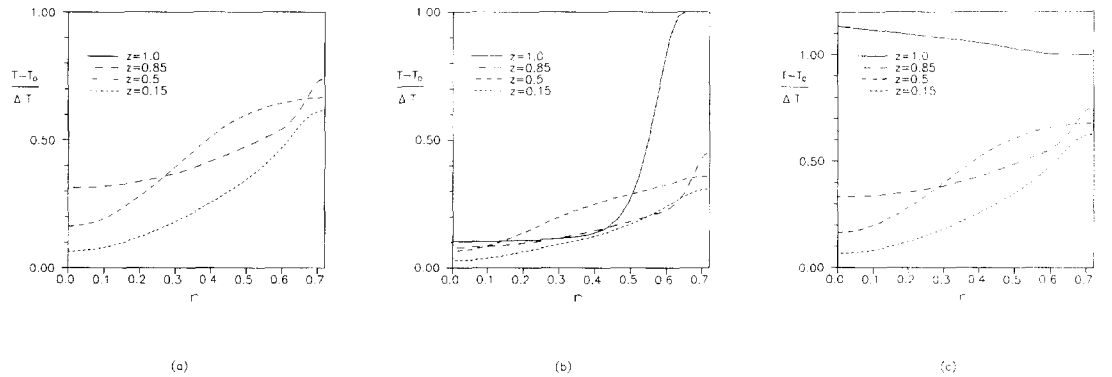

Fig. 5. Temperature distributions along the radial direction with $Pr = 50$, $Ma = 5000$, $A = 0.7$ for: (a) usual half zone model, (b) simulation half zone model and, (c) modified half zone model.

modified half zone model c. The temperature gradient along the radial direction is quite large near the heating source for simulation model b.

Simulation model b has very different profiles of temperature and velocity from the usual model a and modified model c and the results of models a and c are similar. The reason for similar features of models a and c is due to the assumption of a small temperature difference on the upper rod boundary and the assumption is given according to the results of the experiment.

4. CONCLUSIONS

A simulation half zone model has been suggested in this paper and the model relates more closely to the half part of a floating full zone, since the temperature distribution will be symmetric for the middle plan in a floating full zone in a microgravity environment. The temperature distribution has a lower value near the axis than near the free surface at the upper rod boundary. The temperature gradient in the normal direction is zero at the upper rod and the largest temperature gradient in the normal direction exists near the free surface and the rods. The main features of the simulation model suggested in the present paper were studied numerically in detail.

The modified half zone model c is also analyzed in this paper. The modified model c has been suggested experimentally to simulate more closely the half part of a full zone and benefits from the observation of a flow pattern in the transverse cross-section. Since the transparent material has a large thermal conductivity in comparison with the experimental medium such as silicon oil etc., the temperature distribution at the upper rod has the largest value in the central part of the upper rod and the temperature gradient in the axial direction is also large near the axis as in the usual half zone model. However, the temperature condition at the upper rod does not satisfy the condition as given in simulation model b, but is closer to the condition in usual model a. Therefore, the main features of model c are similar to the usual model a, but not the simulation model b.

The main differences in the simulation half zone model b from the usual half zone model a and the modified half zone model c are given in the present simulations in detail. The simulation half zone model has a non-uniform temperature distribution on the upper rod with a low temperature and zero temperature gradient along the longitudinal direction at the upper rod. This model can be used to simulate better the half part of a floating full zone, since the temperature distribution will be symmetric for the middle plane in a full zone in a microgravity environment. Both the usual half zone model and the modified half zone model have nearly uniform or high temperature in the central part of the upper rod and the different applied temperature profiles determine the different features of different sorts of floating half zones. It should be emphasized that every kind of floating half zone contributes to improving the understanding of thermocapillary convection and should be studied in its own right. All the knowledge is helpful to material processing in general. Further experimental studies and three-dimensional linear instability analyses of the simulation half zone model need to be conducted in the future.

Acknowledgements—Hu acknowledges helpful discussions with Professor A. Hirata and his colleagues at Waseda University, who have completed a lot of experiments on the modified simulation model. The idea of the simulation model in the present paper was stimulated when Hu visited Waseda University in the summer of 1995.

REFERENCES

1. Chang, C. E. and Wilcox, W. R., *Journal of Crystal Growth*, 1975, **28,** 8.
2. Chun, C. H. and Wuest, W., *Acta Astronautica*, 1978, **5,** 681.
3. Chun, C. H. *Journal of Crystal Growth*, 1980, **48,** 600.
4. Schwabe D. and Scharmann, A., *Journal of Crystal Growth*, 1979, **46,** 125.
5. Preisser, F., Schwabe, D. and Scharmann, A., *Journal of Fluid Mechanics*, 1983, **126,** 545.
6. Kamotani, Y., Ostrach, S. and Vargas, M., *Journal of Crystal Growth*, 1984, **66,** 83.
7. Hu, W. R., You, H. T. and Cao, C. H., *Science in China: A*, 1992, **4,** 383.
8. Hu, W. R., Shu, J. Z., Zhou, R. and Tang, Z. M., *Journal of Crystal Growth*, 1994, **142,** 379.
9. Hirata, A., Nishizawa, S. and Sakurai, M., *Journal of Japan Society of Microgravity Application*, 1992, **11,** 189.
10. Hirata, A., Nishizawa, S., Noguchi, M., Sakurai, M., Yasuhiro, S. and Imaishi, N., *Journal of Chemical Engineering Japan*, 1994, **27,** 65.
11. Lee, J., Lee, D. J. and Lee, J. H., *Journal of Crystal Growth*, 1995, **152,** 341.
12. Gresho, P. M. and Sani, R. L., *International Journal for Numerical Methods in Fluids*, 1987, **7,** 1111.
13. Gottlieb, D. and Orszag, S. A., NSF-CBMS Monograph No. 26. SIAM, Philadelphia, PA, 1977.
14. Tang, Z. M., Cao, C. Z. and Hu, W. R., *Acta Mechanica Sinica*, 1992, **24,** 411.
15. Hu, W. R. and Tang, Z. M., *Proceedings of the 12th European Symposium on Materials and Fluid Sciences in Microgravity*, Oxford, 1989, p. 279.